

# CLUSTERED GAUSSIAN PROCESS MODEL WITH AN APPLICATION TO SOLAR IRRADIANCE EMULATION

BY CHIH-LI SUNG<sup>\*,¶</sup> BENJAMIN HAALAND<sup>†</sup>  
YOUNGDEOK HWANG<sup>‡</sup> AND SIYUAN LU<sup>§</sup>

*Michigan State University<sup>\*</sup>, University of Utah<sup>†</sup>  
Baruch College, City University of New York<sup>‡</sup>  
IBM Thomas J. Watson Research Center<sup>§</sup>*

A Gaussian process has been one of the important approaches for emulating computer simulations. However, the stationarity assumption for a Gaussian process and the intractability for large-scale dataset limit its availability in practice. In this article, we propose a clustered Gaussian process model which segments the input data into multiple clusters, in each of which a Gaussian process is performed. The stochastic expectation-maximization is employed to efficiently fit the model. In our simulations as well as a real application to solar irradiance emulation, our proposed method had smaller mean square error than its main competitors, with competitive computation time, and provides valuable insights from data by discovering the clusters.

**1. Introduction.** A Gaussian process (GP) has been one of the most popular modeling tools in various research topics, such as spatial statistics (Stein, 2012), computer experiments (Fang, Li and Sudjianto, 2005; Santner, Williams and Notz, 2018), machine learning (Rasmussen and Williams, 2006), and robot control (Nguyen-Tuong and Peters, 2011). Gaussian processes provide the flexibility for a prior probability distribution over functions in Bayesian inference, and its posterior is not only able to estimate the functional for an unseen point but also has uncertainty information. This explicit probabilistic formulation for GP has proved to be powerful for general function learning problems. However, this modeling technique is often limited in the following two applications. First, GP posterior involves  $O(N^3)$  computational complexity and  $O(N^2)$  storage where  $N$  is the sample size, so that it becomes infeasible for large data sets, say  $N = 10^3$ . Second, a GP model often considers a stationary covariance function, in the sense that the outputs with the same separation of any two inputs are assumed to have an equal covariance. We call it a stationary GP in the article. This assumption is violated in many practical applications, particularly for nonstationary processes. Figure 1 demonstrates an illustrative example in Gramacy and Lee (2009) where a stationary GP can perform very poorly when the underlying function indeed consists of

---

<sup>¶</sup>Corresponding author

*Keywords and phrases:* Computer experiments, Nonstationarity, Large-scale dataset, Uncertainty quantification, Mixed models

two different functions: a relatively rough function in the region  $x \in [0, 10]$  and a simple linear function in the region  $x \in [10, 20]$ . Figure 1 shows that a stationary GP results in very poor prediction particularly in the region  $x \in [10, 20]$  with very high uncertainty. See more examples in [Higdon, Swall and Kern \(1999\)](#); [Paciorek and Schervish \(2006\)](#); [Bui-Thanh, Ghattas and Higdon \(2012\)](#).

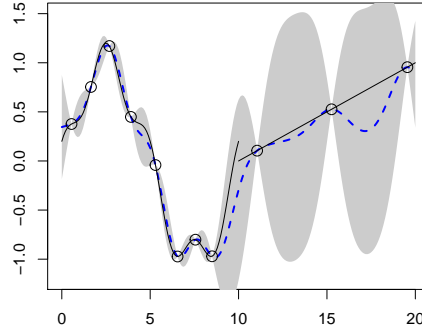


Fig 1: An example of stationary Gaussian processes. Black line is the true function, and black dots represent the collected data. The blue dashed line represent a stationary Gaussian process, with the gray shaded region providing a pointwise 95% confidence band.

These two bottlenecks of GP have attracted lots of attention in recent literatures. To name a few, sparse approximation ([Quiñonero-Candela and Rasmussen, 2005](#); [Sang and Huang, 2012](#)), covariance tapering ([Furrer, Genton and Nychka, 2006](#)), inducing inputs ([Snelson and Ghahramani, 2006](#); [Titsias, 2009](#)), multi-step interpolation ([Haaland and Qian, 2011](#)), special design ([Plumlee, 2014](#)), multi-resolution approximation ([Nychka et al., 2015](#)), address the computational issue for large datasets. For nonstationarity, [Higdon, Swall and Kern \(1999\)](#); [Paciorek and Schervish \(2006\)](#); [Plumlee and Apley \(2017\)](#) adopted nonstationary covariance functions for Gaussian processes. [Tresp \(2001\)](#); [Rasmussen and Ghahramani \(2002\)](#); [Kim, Mallick and Holmes \(2005\)](#); [Gramacy and Lee \(2008\)](#) considered multiple Gaussian processes by segmentation in the input spaces. [Ba and Joseph \(2012\)](#) proposed a composite of two Gaussian processes, which respectively capture a smooth global trend and local details. However, only few of them are able to tackle the nonstationarity and computational issues simultaneously. Exceptions include the multi-resolution functional ANOVA approximation ([Sung et al., 2019](#)) which uses group lasso algorithm to identify important basis functions, and the local Gaussian process approximation which selects a small subsample to fit a Gaussian process model for each predictive location ([Gramacy and Apley, 2015](#)).

In this article, we propose a clustered Gaussian process (clustered GP) to resolve

the two bottlenecks simultaneously. The clustered GP is along the line of the idea of input segmentation, considering multiple Gaussian processes in the input spaces, but incorporates with the traditional hard-assignment clustering approaches, such as  $K$ -means clustering. This makes the computation more tractable and flexible for large datasets, and also provides some valuable insights from the data by seeing what groups the data points fall into. Unlike traditional clustering approaches, the clustered GP is supervised learning because the assignments to each cluster need to be trained by inputs and outputs, which makes this problem more challenging.

The remainder of this article is organized as follows. In Section 2, the clustered GP model is explicitly described, including the relationship with the existing methods. In Section 3, a stochastic expectation-maximization algorithm is introduced to fit the clustered GP model. In Section 4, we introduce how to predict responses at new locations based on a clustered GP model. Some computational details are discussed in Section 5. In Section 6, some synthetic examples are demonstrated to show the tractability and the prediction performance of the proposed method. A real data application for predicting solar irradiance over the United States is presented in Section 7. Some potential future work is discussed in Section 8. Mathematical proof, explicit algorithm, and further examples are given in Appendix.

## 2. Clustered Gaussian Process.

**2.1. Preliminary: Gaussian Processes.** A brief review for Gaussian processes is first given in this section. A Gaussian process is a stochastic process whose finite dimensional distributions are defined via a mean function  $\mu(x)$  and a covariance function  $\Sigma(x, x')$  for  $d$ -dimensional  $x, x' \in \chi \subseteq \mathbb{R}^d$ . If the function  $y(\cdot)$  is a draw from a Gaussian process, then we write

$$y(\cdot) \sim \mathcal{GP}(\mu(\cdot), \Sigma(\cdot, \cdot)).$$

In particular, given  $n$  inputs  $X = (x_1, \dots, x_n)$ , if  $y(\cdot)$  is a Gaussian process, then the outputs  $Y = (y(x_1), \dots, y(x_n))$  have a multivariate normal distribution

$$Y|X \sim \mathcal{N}(\mu(X), \Sigma(X, X)),$$

where  $\mu(X) \in \mathbb{R}^n$  and  $\Sigma(X, X) \in \mathbb{R}^{n \times n}$  are defined as  $(\mu(X))_i = \mu(x_i)$  and  $(\Sigma(X, X))_{i,j} = \Sigma(x_i, x_j)$ , respectively. Conventionally,  $\mu(\cdot)$  is often assumed to be a constant mean, i.e.,  $\mu(\cdot) = \mu$ , and  $\Sigma(\cdot, \cdot)$  is assumed to have the form  $\sigma^2 \Phi_\gamma(\cdot, \cdot)$ , where  $\Phi_\gamma$  is a correlation function with  $\Phi_\gamma(x, x) = 1$  for any  $x \in \chi$  and contains the unknown parameter  $\gamma$ . In addition,  $\Phi_\gamma$  is often assumed to depend on the displacement between two input locations, that is,  $\Phi_\gamma(x, x') = R(x - x')$  for some positive-definite function  $R$ . Such a correlation function is called *stationary* correlation function which implies the process  $y(\cdot)$  is stationary, since

$y(x_1), \dots, y(x_L)$  and  $y(x_1 + h), \dots, y(x_L + h)$  have the same distribution for any  $h \in \mathbb{R}^d$  and  $x_1, \dots, x_L, x_1 + h, \dots, x_L + h \in \chi$ . A common choice for  $\Phi$  is a power correlation function

$$(1) \quad \Phi_\gamma(x, x') = \exp\{-\|\gamma^T(x - x')\|^p\},$$

where  $p$  is often fixed to control the smoothness of the output surface, and  $\gamma = (\gamma_1, \dots, \gamma_d)^T$  controls the decay of correlation with respect to the distance between  $x$  and  $x'$ . Hence, the parameters include  $\mu(\cdot)$ ,  $\sigma^2$  and  $\gamma$  and can be estimated by either maximum likelihood estimation or Bayesian estimation. See [Fang, Li and Sudjianto \(2005\)](#), [Rasmussen and Williams \(2006\)](#) and [Santner, Williams and Notz \(2018\)](#) for more details. Importantly, when the interest is in the prediction at an untried  $x_{\text{new}}$ , whose response could be denoted as  $y_{\text{new}}$ , the predictive distribution of  $y_{\text{new}}$  can be derived by the conditional multivariate normal distribution. In particular, one can show that  $y_{\text{new}}|Y, X, x_{\text{new}} \sim \mathcal{N}(\mu^*, (\sigma^*)^2)$ , where

$$(2) \quad \mu^* = \mu(x_{\text{new}}) + \Phi_\gamma(x_{\text{new}}, X)\Phi_\gamma(X, X)^{-1}(Y - \mu(X)),$$

and

$$(3) \quad (\sigma^*)^2 = \sigma^2 (1 - \Phi_\gamma(x_{\text{new}}, X)\Phi_\gamma(X, X)^{-1}\Phi_\gamma(X, x_{\text{new}})).$$

In practice, the unknown parameters  $\mu(\cdot)$ ,  $\sigma^2$  and  $\gamma$  in (2) and (3) are replaced by their estimates.

**2.2. Clustered Gaussian Process.** In general, we might expect the unknown function that we are trying to approximate to exhibit some degree of non-stationarity. A natural conceptual model would be a mixture Gaussian process, where the components of the mixture represent high-quality models for subsets of the data which are approximately stationary. That is,

$$(4) \quad \begin{aligned} y(\cdot) | z(\cdot) = k &\sim \mathcal{GP}(\mu_k(\cdot), \sigma_k^2 \Phi_{\gamma_k}(\cdot, \cdot)), \quad k = 1, \dots, K, \\ \Pr(z(x) = k) &= g_k(x; \varphi_k), \quad k = 1, \dots, K, \end{aligned}$$

where  $\mu_k(\cdot)$ ,  $\sigma_k^2$  and  $\Phi_{\gamma_k}$  are the mean function, variance, and stationary correlation function of the  $k$ -th Gaussian process, and  $g_k(x, \varphi_k)$  is the probability that  $z(x) = k$  with unknown parameter  $\varphi_k$  satisfying  $\sum_{k=1}^K g_k(x; \varphi_k) = 1$  for any  $x$ . The choice for  $g_k$  will be greatly discussed in Section 5.1. It can be seen that in this model,  $z(\cdot)$  plays the role of a latent function, which assigns  $y(\cdot)$  to the  $k$ -th Gaussian process, or cluster  $k$ . These assignments introduce non-stationarity to the response  $y(\cdot)$ , even though each Gaussian process is stationary.

Now, a little notation is first introduced. Given  $n$  inputs  $X = (x_1, \dots, x_n)$ , denote the corresponding outputs as  $Y = (Y(x_1), \dots, Y(x_n))$ . For cluster  $k =$

$1, \dots, K$ , let  $\mathcal{P}_k = \{i : z(x_i) = k\}$  denote the set of indices of the observations in cluster  $k$ . Additionally, let  $Y_{\mathcal{P}_k}$  and  $X_{\mathcal{P}_k}$  respectively denote the (ordered) responses and input locations for the observations from cluster  $k$ . Then, given  $Z = (z_1, \dots, z_n) \equiv (z(x_1), \dots, z(x_n))$ , the output  $Y_{\mathcal{P}_k}$  in each cluster  $k$  has the multivariate normal distribution

$$(5) \quad Y_{\mathcal{P}_k} | X_{\mathcal{P}_k} \sim \mathcal{N}(\mu_k(X_{\mathcal{P}_k}), \sigma_k^2 \Phi_{\gamma_k}(X_{\mathcal{P}_k}, X_{\mathcal{P}_k})).$$

A straight-forward application of a likelihood-based approach to estimate the unknown parameters, however, is quite cumbersome, mainly due to strong dependencies among observations and computational challenges. Suppose, that one models the latent cluster/mixture component assignments  $z_i$  as independent across observations  $i$  and potentially depending on input location  $x_i$ , so that the (unobserved) cluster assignment likelihood is

$$(6) \quad \begin{aligned} f(Z|X) &= \Pr(z(x_1) = z_1, \dots, z(x_n) = z_n) \\ &= \prod_{i=1}^n g_{z_i}(x_i; \varphi_{z_i}) = \prod_{k=1}^K \prod_{i \in \mathcal{P}_k} g_k(x_i; \varphi_k). \end{aligned}$$

Within each cluster, on the other hand, as shown in (5), the observed  $y_i$ 's depend on the response values and locations of the other cluster members, in addition to their corresponding input location  $x_i$ . Then, by combining (5) and (6), the likelihood function of complete data is

$$(7) \quad \begin{aligned} f(Y, Z|X) &= f(Y|X, Z) f(Z|X) \\ &= \left( \prod_{k=1}^K f_k(Y_{\mathcal{P}_k} | X_{\mathcal{P}_k}; \theta_k) \right) \left( \prod_{k=1}^K \prod_{i \in \mathcal{P}_k} g_k(x_i; \varphi_k) \right), \end{aligned}$$

where  $f_k$  is the probability density function of a multivariate normal distribution with parameters  $\theta_k \equiv \{\mu_k(\cdot), \sigma_k^2, \gamma_k\}$ .

An intuitive next step towards using this type of model would be to compute the cluster probabilities  $f(Z|X, Y)$ , whether for implementing the E-step in the EM algorithm (soft assignment) or updating cluster membership in a  $K$ -means type algorithm (hard assignment). Unfortunately, the cluster probability  $f(Z|X, Y)$  do not factor beyond being proportional to (7), so we cannot compute the cluster memberships for each observation separately from one another. Instead, a stochastic EM algorithm (Celeux and Diebolt, 1985) will be applied here, which is known to avoid insignificant local maxima of likelihood functions, and it turns out that it will lead to a computationally efficient algorithm. This will be explicitly introduced in Section 3.

**2.3. Related Work.** The clustered GP is closely related to some of existing methods. For example, if  $z(\cdot)$  is a Bayesian treed models, the model becomes close to the Bayesian treed Gaussian process model of [Gramacy and Lee \(2008\)](#). If  $z(\cdot)$  assigns cluster memberships based on a Voronoi tessellation, the model bears some similarity to the model of [Kim, Mallick and Holmes \(2005\)](#). If  $z(\cdot)$  is a Dirichlet process or a generalized Gaussian process, the model then has a similar flavor to the mixtures of Gaussian processes of [Tresp \(2001\)](#) and [Rasmussen and Ghahramani \(2002\)](#), respectively. Despite successful applications of these models, the application for large-scale data is not clear. In the next section, a stochastic EM algorithm is employed for fitting a clustered GP model which enjoys computational efficiency even for large-scale data.

### 3. Stochastic EM Algorithm.

**3.1. Stochastic E-step.** In the EM-algorithm, the E-step computes the expected value of the log posterior of complete data given the observed data  $Y$ :

$$(8) \quad \mathbb{E}[\log f(Y, Z|X)|X, Y] + \log \pi(\boldsymbol{\theta}) + \log \pi(\boldsymbol{\varphi}),$$

where  $\boldsymbol{\theta} = \{\theta_k\}_{k=1}^K$ ,  $\boldsymbol{\varphi} = \{\varphi_k\}_{k=1}^K$ , and  $\pi(\boldsymbol{\theta})$  and  $\pi(\boldsymbol{\varphi})$  are priors of  $\boldsymbol{\theta}$  and  $\boldsymbol{\varphi}$ . We assume  $\theta_k$  and  $\varphi_k$  are mutually independent through  $k = 1, \dots, K$  so

$$(9) \quad \log \pi(\boldsymbol{\theta}) = \sum_{k=1}^K \log \pi(\theta_k) \quad \text{and} \quad \log \pi(\boldsymbol{\varphi}) = \sum_{k=1}^K \log \pi(\varphi_k).$$

Computing the expected value requires the computation of the cluster probabilities  $f(Z|X, Y)$ , which, unfortunately, cannot be computed explicitly. Instead, we consider adopting a Gibbs sampling, or iterative stochastic hard assignment, perspective. The key quantity for this approach is the cluster membership probability for observation  $i$  given the data  $X, Y$  and the other cluster memberships  $Z_{-i}$ ,

$$(10) \quad \begin{aligned} f(z_i = k|X, Y, Z_{-i}) &\propto f(Y|X, Z_{-i}, z_i = k)f(z_i = k|X, Z_{-i}) \\ &= \left( f_k(Y_{\mathcal{P}_k \cup \{i\}}|X_{\mathcal{P}_k \cup \{i\}}; \theta_k) \prod_{j \neq k} f_j(Y_{\mathcal{P}_j \setminus \{i\}}|X_{\mathcal{P}_j \setminus \{i\}}; \theta_j) \right) \Pr(z_i = k) \\ &= \left( f_k(Y_{\mathcal{P}_k \cup \{i\}}|X_{\mathcal{P}_k \cup \{i\}}; \theta_k) \prod_{j \neq k} f_j(Y_{\mathcal{P}_j \setminus \{i\}}|X_{\mathcal{P}_j \setminus \{i\}}; \theta_j) \right) g_k(x_i; \varphi_k). \end{aligned}$$

The second equation holds since  $z_i$  is independent across observations  $i$ . In fact, (10) can be simplified quite nicely even in this highly dependent situation. See proposition [3.1.1](#), whose proof is given in Appendix [A](#).

PROPOSITION 3.1.1. *Under the complete data likelihood given in (7),*

$$(11) \quad f(z_i = k|X, Y, Z_{-i}) \propto \phi((y_i - \mu_k^*)/\sigma_k^*)g_k(x_i; \varphi_k), \quad \text{where}$$

(12)

$$\begin{aligned} \mu_k^* &= \mu_k(x_i) + \Phi_{\gamma_k}(x_i, X_{\mathcal{P}_k \setminus \{i\}}) \Phi_{\gamma_k}(X_{\mathcal{P}_k \setminus \{i\}}, X_{\mathcal{P}_k \setminus \{i\}})^{-1} (Y_{\mathcal{P}_k \setminus \{i\}} - \mu_k(X_{\mathcal{P}_k \setminus \{i\}})), \\ (\sigma_k^*)^2 &= \sigma_k^2 (1 - \Phi_{\gamma_k}(x_i, X_{\mathcal{P}_k \setminus \{i\}}) \Phi_{\gamma_k}(X_{\mathcal{P}_k \setminus \{i\}}, X_{\mathcal{P}_k \setminus \{i\}})^{-1} \Phi_{\gamma_k}(X_{\mathcal{P}_k \setminus \{i\}}, x_i)), \end{aligned}$$

where  $\phi$  denotes the density probability function of a standard normal distribution.

The result indeed has an intuitive explanation. Suppose  $x_i$  is an unknown predictive location. Then, the predictive distribution of each cluster  $k$  has a normal distribution with mean  $\mu_k^*$  and variance  $(\sigma_k^*)^2$  as in (2) and (3). Thus, the membership of  $z_i$  then can be determined by the probability density function of cluster  $k$  at  $y_i$ , and the probability mass function  $g_k$  of membership  $k$  at  $x_i$ . If  $y_i$  is closer to  $\mu_k^*$  with the scale  $\sigma_k^*$ , or  $g_k$  has a high mass probability at location  $x_i$ , then  $z_i$  is more likely to be assigned to class  $k$ .

Mechanically, one could loop through observation  $i$  repeatedly, by first computing probabilities proportional to the above  $K$  quantities for each, and then by drawing a random multinomial cluster assignment. Importantly, each step of this Gibbs scheme satisfies detailed balance (assuming none of the probabilities/densities in (11) equal zero), so eventually this process produces samples from  $f(Z|X, Y)$ . Then, the cluster membership samples can be used to approximate quantities depending on  $f(Z|X, Y)$  such as the expectation in (8). Further, partitioned matrix inverse and determinant formulas (Harville, 1998) allow one to update the augmented and diminished Gaussian densities in  $O(n_k^2)$  time, where  $n_k$  denotes the number of observations in cluster  $k$ . In total, each sweep through the observations would take at most  $O(\sum_{k=1}^K n_k^3)$ . To ease computational burden, one may consider setting a maximum number of observations in each cluster, denoted by  $n_{\max}$ , then the computation becomes  $O(Kn_{\max}^3)$  in total. A straight-forward idea is to force the probabilities/densities equal zero when  $n_k > n_{\max}$ . An important aspect of this step is that it can be easily parallelized. The computation of (12) for each  $k$  can be distributed over multiple cores. The algorithm is given in Stochastic E-step of Appendix B.

3.2. *M-step.* Denote  $\tilde{Z}$  as the assignments for  $Z$  given in the stochastic E-step and let  $\tilde{\mathcal{P}}_k = \{i : \tilde{z}_i = k\}$  denote the set of indices of the observations in cluster  $k$ , the log posterior of complete data (8) is approximately by

$$\begin{aligned} & \log f(Y, \tilde{Z}|X) + \log \pi(\boldsymbol{\theta}) + \log \pi(\boldsymbol{\varphi}) \\ &= \sum_{k=1}^K \log f_k(Y_{\tilde{\mathcal{P}}_k} | X_{\tilde{\mathcal{P}}_k}; \theta_k) + \sum_{k=1}^K \sum_{i \in \tilde{\mathcal{P}}_k} \log g_k(x_i; \varphi_k) + \sum_{k=1}^K \log \pi(\theta_k) + \sum_{k=1}^K \log \pi(\varphi_k). \end{aligned}$$

The equation is from (7) and (9). The maximum a posteriori probability (MAP) estimate  $\{\hat{\theta}_k\}_{k=1}^K$  and  $\{\hat{\varphi}_k\}_{k=1}^K$  can then be obtained by maximizing

$$\sum_{k=1}^K \log \left( f_k(Y_{\tilde{\mathcal{P}}_k} | X_{\tilde{\mathcal{P}}_k}; \theta_k) \pi(\theta_k) \right) \quad \text{and} \quad \sum_{k=1}^K \left( \sum_{i \in \tilde{\mathcal{P}}_k} \log g_k(x_i; \varphi_k) + \log \pi(\varphi_k) \right),$$

respectively. In particular,  $\sum_{k=1}^K \log \left( f_k(Y_{\tilde{\mathcal{P}}_k} | X_{\tilde{\mathcal{P}}_k}; \theta_k) \pi(\theta_k) \right)$  can be optimized by maximizing each component  $f_k(Y_{\tilde{\mathcal{P}}_k} | X_{\tilde{\mathcal{P}}_k}; \theta_k) \pi(\theta_k)$ , which is proportional to the posterior distribution of the  $k$ -th Gaussian process. The choice for the prior of  $\theta_k$  and its posterior can be found in Chapter 3 and 4 of [Santner, Williams and Notz \(2018\)](#). The computation for M-step for  $K$  clusters also can be easily parallelized similarly to the E-step. The explicit algorithm is given in Appendix B.

**3.3. Frequentist version.** One may consider a frequentist version of stochastic EM by replacing MAP estimation with maximum likelihood (ML) estimation, or simply by letting the prior distributions of  $\{\theta_k\}_{k=1}^K$  and  $\{\varphi_k\}_{k=1}^K$  be uniform. By doing so, under some regularity conditions the ML estimators  $\{\hat{\theta}_k\}_{k=1}^K$  and  $\{\hat{\varphi}_k\}_{k=1}^K$  can be shown to have an asymptotically normal distribution. We refer the asymptotic properties of the parameter inference to [Nielsen et al. \(2000\)](#).

**4. Prediction.** Predicting the responses  $y_{\text{new}}$  at a new location  $x_{\text{new}}$  can be challenging, since the cluster assignment  $z_{\text{new}}$  at the new location is unknown. Given the assignment  $\hat{Z} = (\hat{z}(x_1), \dots, \hat{z}(x_n))$  and the estimates  $\{\hat{\theta}_k, \hat{\varphi}_k\}_{k=1}^K$  returned in the stochastic EM algorithm, we perform the predictive distribution of  $y_{\text{new}}$  by weighted averaging across the clustered GPs:

$$\begin{aligned} f(y_{\text{new}} | x_{\text{new}}, X, Y, \hat{Z}) &= \sum_{k=1}^K f(y_{\text{new}} | z_{\text{new}} = k, x_{\text{new}}, X, Y, \hat{Z}) f(z_{\text{new}} = k | x_{\text{new}}, X, Y, \hat{Z}) \\ &= \sum_{k=1}^K \phi((y_{\text{new}} - \hat{\mu}_k^*) / \hat{\sigma}_k^*) g_k(x_{\text{new}}; \hat{\varphi}_k), \end{aligned}$$

where

$$\begin{aligned} \hat{\mu}_k^* &= \hat{\mu}_k(x_{\text{new}}) + \Phi_{\hat{\gamma}_k}(x_{\text{new}}, X_{\hat{\mathcal{P}}_k}) \Phi_{\hat{\gamma}_k}(X_{\hat{\mathcal{P}}_k}, X_{\hat{\mathcal{P}}_k})^{-1} \left( Y_{\hat{\mathcal{P}}_k} - \hat{\mu}_k(X_{\hat{\mathcal{P}}_k}) \right), \\ (\hat{\sigma}_k^*)^2 &= \hat{\sigma}_k^2 \left( 1 - \Phi_{\hat{\gamma}_k}(x_{\text{new}}, X_{\hat{\mathcal{P}}_k}) \Phi_{\hat{\gamma}_k}(X_{\hat{\mathcal{P}}_k}, X_{\hat{\mathcal{P}}_k})^{-1} \Phi_{\hat{\gamma}_k}(X_{\hat{\mathcal{P}}_k}, x_{\text{new}}) \right). \end{aligned}$$

Thus, the prediction mean of  $y_{\text{new}}$  is

$$(13) \quad \hat{y}_{\text{new}} := \mathbb{E}[y_{\text{new}} | x_{\text{new}}, X, Y, \hat{Z}] = \sum_{k=1}^K \hat{\mu}_k^* g_k(x_{\text{new}}; \hat{\varphi}_k),$$



with its variance

$$\begin{aligned}\mathbb{V}[y_{\text{new}}|x_{\text{new}}, X, Y, \hat{Z}] &= \mathbb{E}[\mathbb{V}[y_{\text{new}}|z_{\text{new}}, x_{\text{new}}, X, Y, \hat{Z}]] + \mathbb{V}[\mathbb{E}[y_{\text{new}}|z_{\text{new}}, x_{\text{new}}, X, Y, \hat{Z}]] \\ &= \sum_{k=1}^K (\hat{\sigma}_k^*)^2 g_k(x_{\text{new}}; \hat{\varphi}_k) + \sum_{k=1}^K (\hat{\mu}_k^*)^2 g_k(x_{\text{new}}; \hat{\varphi}_k) - \left( \sum_{k=1}^K \hat{\mu}_k^* g_k(x_{\text{new}}; \hat{\varphi}_k) \right)^2.\end{aligned}$$

The  $q$ -th quantile of  $y_{\text{new}}$ , which will be used for constructing confidence intervals, has no closed form but can be calculated by finding the value of  $y$  for which  $\int_{-\infty}^y f(t|x_{\text{new}}, X, Y, \hat{Z})dt = q$ , which is equivalent to solving

$$\sum_{k=1}^K \left( \int_{-\infty}^y \phi((t - \hat{\mu}_k^*)/\hat{\sigma}_k^*)dt \right) g_k(x_{\text{new}}; \hat{\varphi}_k) = q.$$

The summation and integration are interchangeable because the probability density function is finite. The equation can be solved numerically, such as using a line search.

It should be noted that the stochastic EM and prediction can be modified in a fully Bayesian fashion, that is, using the Monte Carlo samples from the posterior distribution of  $\{z(x_i)\}_{i=1}^n, \{\theta_k, \varphi_k\}_{k=1}^K$  with a Gibbs routine to generate predictions. This idea, however, can be difficult to apply in a large-data context without substantial modification due to the computational burden. In particular, saving samples from the posteriors requires enormous amounts of storage for large data sets. Therefore, the returned assignment  $\hat{Z}$  and the MAPs  $\{\hat{\theta}_k, \hat{\varphi}_k\}_{k=1}^K$  are used as representative samples which is more efficient for both fitting and prediction procedures.

## 5. Computational details.

**5.1. Modeling  $z(\cdot)$ .** The model for  $z(\cdot)$  in (4) provides the latent class distribution of the cluster assignment, where  $g_k$  is the conditional probability that  $z(x) = k$  given an input  $x$ . One can consider a  $K$ -class multinomial logistic regression,

$$\Pr(z(x) = k) = g_k(x; \varphi_k) = \frac{\exp\{\beta_{0,k} + \beta_k^T x\}}{\sum_{j=1}^K \exp\{\beta_{0,j} + \beta_j^T x\}},$$

for  $k = 1, \dots, K-1$  and  $\Pr(z(x) = K) = 1 - \sum_{j=1}^{K-1} \Pr(z(x) = j)$ , where  $\beta_{0,k}$  is the intercept,  $\beta_k$  is a  $d$ -dimensional coefficient of  $x$ , and  $\varphi_k = (\beta_{0,k}, \beta_k)$ . Alternatively, one can also consider the linear discriminant analysis (LDA) or quadratic discriminant analysis (QDA) methods by assuming

$$g_k(x; \varphi_k) = \phi(x; \nu_k, \Sigma_k) \quad \text{for } k = 1, \dots, K,$$

where  $\phi(x; \nu_k, \Sigma_k)$  is the density probability function of a (multivariate) normal distribution with mean  $\nu_k$  and covariance  $\Sigma_k$ . LDA assumes  $\Sigma_1 = \dots = \Sigma_K$ , while QDA assumes the covariances can be different. The multinomial logistic regression and LDA methods are indeed closely connected, which often result in similar linear decision boundaries of the  $K$  classes. QDA methods, on the other hand, result in quadratic decision boundaries. From our preliminary investigation, the clustered Gaussian processes with these models give similar prediction results. To save space, only  $K$ -class multinomial logistic regression is presented in the sections of numerical study and solar irradiance prediction (Sections 6 and 7).

**5.2. Initialization.** The stochastic EM algorithm can be sensitive to the initialization. One may run many initializations and select the one that gives the optimal criterion. This is, however, computationally intensive especially for large data sets. One potential initialization is the  $K$ -means clusters or other unsupervised clustering algorithms which are solely determined by the input  $X$ . This initialization enables the clustered GP to make the input locations of each cluster close to each other and distant from the ones of other clusters, which often leads to nice model interpretation. Although this initialization may end up with a local optimum, our preliminary investigation showed that the clustered GPs based on the initialization often result in promising prediction accuracy along with nice model interpretation. In Sections 6 and 7, the initialization of  $K$ -means clusters will be used.

**5.3. Stopping rule.** The iteration in the stochastic EM algorithm (Appendix B) stops until the cluster assignments stop changing or some criterion converges. One criterion that can be used is the cross-validated prediction error, such as 10-fold cross-validation (CV) or leave-one-out cross-validation (LOOCV). For instance, LOOCV iteratively holds out one particular location, trains on the data remaining at other locations, and then makes prediction for the held-out location. However, these cross-validated prediction errors have potential to be expensive to implement, since the model has to fit 10 times (10-fold CV) or  $n$  times (LOOCV) in each iteration. Fortunately, the clustered GP has a shortcut that makes the cost of LOOCV much cheaper. Specifically, denote  $\tilde{y}_i$  as the prediction mean based on all data except  $i$ -th observation and  $y_i$  as the real output of  $i$ -th observation, then based on (13),

$$\tilde{y}_i = \sum_{k=1}^K \hat{\mu}_k^{(-i)} g_k(x_i; \hat{\varphi}_k),$$

where

(14)

$$\hat{\mu}_k^{(-i)} = \hat{\mu}_k(x_i) + \Phi_{\hat{\gamma}_k}(x_i, X_{\hat{\mathcal{P}}_k \setminus \{i\}}) \Phi_{\hat{\gamma}_k}(X_{\hat{\mathcal{P}}_k \setminus \{i\}}, X_{\hat{\mathcal{P}}_k \setminus \{i\}})^{-1} \left( Y_{\hat{\mathcal{P}}_k \setminus \{i\}} - \hat{\mu}_k(X_{\hat{\mathcal{P}}_k \setminus \{i\}}) \right).$$

For those  $i$ s which do not belong to  $\hat{\mathcal{P}}_k$ , (14) becomes

$$\hat{\mu}_k^{(-i)} = \hat{\mu}_k(x_i) + \Phi_{\hat{\gamma}_k}(x_i, X_{\hat{\mathcal{P}}_k}) \Phi_{\hat{\gamma}_k}(X_{\hat{\mathcal{P}}_k}, X_{\hat{\mathcal{P}}_k})^{-1} \left( Y_{\hat{\mathcal{P}}_k} - \hat{\mu}_k(X_{\hat{\mathcal{P}}_k}) \right),$$

and for those  $i$ s which belong to  $\hat{\mathcal{P}}_k$ , (14) can be simplified to

$$\hat{\mu}_k^{(-i)} = \hat{\mu}_k(x_i) - \frac{1}{q_{ii}} \sum_{j \neq i}^{n_k} q_{ij} (y_j - \hat{\mu}_k(x_j)),$$

where  $q_{ij}$  is the  $(i, j)$ -th element of  $\Phi_{\hat{\gamma}_k}(X_{\hat{\mathcal{P}}_k}, X_{\hat{\mathcal{P}}_k})^{-1}$ . Then, the LOOCV root-mean-squared error (RMSE) is

$$\sqrt{\frac{1}{n} \sum_{i=1}^n (y_i - \tilde{y}_i)^2} = \sqrt{\frac{1}{n} \sum_{i=1}^n \left( y_i - \sum_{k=1}^K \hat{\mu}_k^{(-i)} g_k(x_i; \hat{\varphi}_k) \right)^2}.$$

This computation costs at most  $O(K n_{\max}^3)$ , which is same as the stochastic E-step.

**5.4. The choice of  $K$ .** The number of clusters  $K$  plays an important role for the degree of non-stationarity of approximation functions which may affect approximation accuracy. A natural choice is using cross-validation with different  $K$ 's to target a small prediction error, such as the LOOCV RMSE described in Section 5.3. Other choices using bootstrap techniques to estimate prediction error also can be considered, such as the 632+ bootstrap method of [Efron and Tibshirani \(1997\)](#). [Kohavi \(1995\)](#) explicitly discussed the comparison between cross-validation and bootstrap from bias and variance point of view and comprehensive numerical experiments were conducted therein. For the purpose of saving computational cost, we target a lowest LOOCV RMSE to choose the best  $K$ , as described in 5.3 that LOOCV RMSE can be computed efficiently for clustered GPs.

**6. Numerical study.** We start with three exemplar functions with one-dimensional input and one with two-dimensional input in Section 6.1 and 6.2, to demonstrate clustered Gaussian processes and visually illustrate the benefit from non-stationary modeling. Then, in section 6.3 the clustered GP is applied to a 8-dimensional function with larger-size synthetic data. The  $K$ -means clusters are chosen as the initialization in all the examples, and the  $K$ -class multinomial logistic regression is modeled for  $z(\cdot)$ . The iteration in the stochastic EM algorithm stops when the number of iterations exceeds 100. We select the assignment  $\hat{Z}$  which results in the lowest LOOCV RMSE during the iterations, which will be illustrated in Section 6.2. Power correlation function of (1) with  $p = 2$  is chosen. In addition, we let the prior distributions of  $\{\theta_k\}_{k=1}^K$  and  $\{\varphi_k\}_{k=1}^K$  be uniform, in which case the inference developed herein is identical to the frequentist inference.

6.1. *One-dimensional synthetic data.* We first consider an example from [Gramacy and Lee \(2009\)](#), which is a modification to the example in [Higdon et al. \(2002\)](#). Suppose the true function is

$$f(x) = \begin{cases} \sin(0.2\pi x) + 0.2 \cos(0.8\pi x), & \text{if } x < 10. \\ 0.1x - 1, & \text{otherwise} \end{cases}$$

and 11 unequally spaced points from  $[0, 20]$  are chosen. The black lines in Figure 2 demonstrate this function, and it can be seen that the function is discontinuous at  $x = 10$ . When the data are fitted by a stationary Gaussian process with a Gaussian correlation function, it can be seen in the left panel of Figure 2 that the prediction within region  $[10, 20]$  performs very badly with large uncertainty. [Ba and Joseph \(2012\)](#) explained that the constant mean assumption for GP is violated so the predictor tends to revert to the global mean, whose estimate is 0.208 by maximum likelihood estimation in this example. This consequence is frequently observed especially at the locations far away from input locations. Moreover, the constant variance assumption for GP is also violated. The function in the region  $[0, 10]$  is rougher than that in the region  $[10, 20]$ . Therefore, the variance estimate for region  $[10, 20]$  tends to be inflated by averaging with that of region  $[0, 10]$ , which leads to the erratic prediction in this region. On the other hand, clustered GP introduces some degree of non-stationarity by considering a mixture GP, which is shown in the right panel of Figure 2. Two subsets of the data are represented as red and green dots, which are given by the assignment  $\hat{Z}$  returned in the stochastic EM algorithm, and both are fitted by stationary GPs. The mean estimates of the GPs are -0.045 and 0.529, respectively. It can be seen that the predictor performs much better than a stationary GP, especially at the locations within region  $[10, 20]$ , in terms of prediction accuracy and uncertainty quantification. The most uncertain region is located on the boundary of two clusters, which is expected because the assignment of cluster membership is more uncertain in the region. One potential remedy of improving the accuracy on the boundaries will be discussed in Section 8.

Two more one-dimensional synthetic data generated from the exemplar functions of [Xiong et al. \(2007\)](#) and [Montagna and Tokdar \(2016\)](#) are presented in Appendix C, in which both examples show that the clustered GP yields better prediction accuracy than a stationary GP.

6.2. *Two-dimensional synthetic data.* In this section, the selection of  $K$  and the stopping rule using LOOCV RMSE will be demonstrated. Consider a wavy function, which also appeared in [Ba and Joseph \(2012\)](#) and [Montagna and Tokdar \(2016\)](#). The wavy function is

$$f(x_1, x_2) = \sin\left(\frac{1}{x_1 x_2}\right),$$

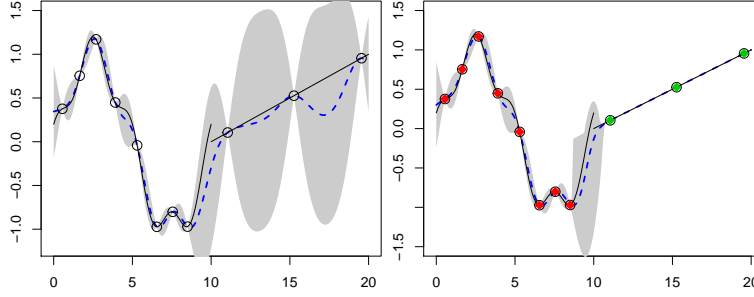


Fig 2: One-dimensional synthetic data. The left and right panels illustrate predictors by a stationary Gaussian process and a clustered Gaussian process, respectively. Black line is the true function, black circles are input locations, and blue dotted lines are the predictors, with the gray shaded region providing a pointwise 95% confidence band. Red and green dots in the right panel represent two different clusters.

where  $x_1, x_2 \in [0.3, 1]$ . The function is illustrated in the left panel of Figure 3, in which it fluctuates rapidly when  $x_1$  and  $x_2$  are small and gets smoother as they increase toward 1. A 40-run maximin distance Latin hypercube design (Morris and Mitchell, 1995) from  $[0.3, 1]^2$  is chosen to select the input locations at which the wavy function is evaluated. These locations are shown as black dots. A stationary GP and a clustered GP with  $K = 3$  are performed on these locations, whose predictive surfaces are shown in the middle and right panels of Figure 3. It can be seen that the stationary GP performs fairly poorly as  $x_1$  and  $x_2$  are small, while the clustered GP generally has better prediction performance over the input space. To evaluate the prediction performance quantitatively, we predict the responses at 1296 ( $= 36 \times 36$ ) equally spaced points from  $[0.3, 1]^2$  as the test points, and compute their RMSEs, that is,

$$\left( \frac{1}{n_{\text{test}}} \sum_{i=1}^{n_{\text{test}}} \left( f(x_1, x_2) - \hat{f}(x_1, x_2) \right)^2 \right)^{1/2},$$

where  $n_{\text{test}}$  is the number of test points and  $\hat{f}(x_1, x_2)$  is the predicted value at  $x_1$  and  $x_2$ . In this example, the clustered GP outperforms the stationary GP in terms of prediction accuracy, where their RMSEs are 0.1872 and 0.3569, respectively.

Figure 4 demonstrates the stopping rule and the selection of  $K$  discussed in Section 5. The left panel presents the LOOCV RMSEs of  $K = 2, 3, 4$  and 5 during the 100 iterations of the stochastic EM algorithm. It shows that even though the LOOCV RMSE of initial iteration of  $K = 3$  is larger than other choices of  $K$ , the error drops rapidly and ends up with a lower LOOCV error at 88-th iteration.

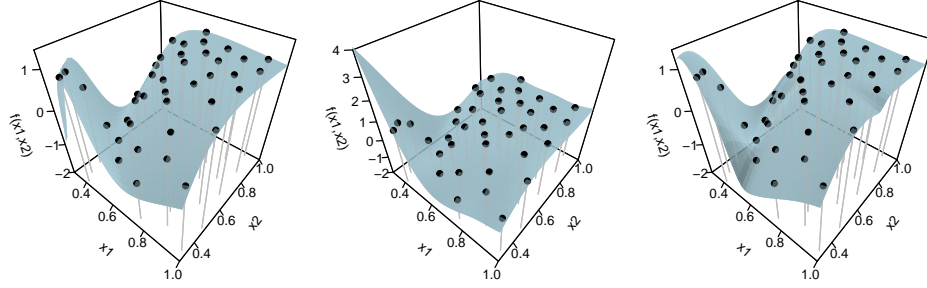


Fig 3: Two-dimensional wavy function, and the input locations which are shown as black dots. The left panel is the true wavy function, the middle panel is the predictive surface of a stationary Gaussian process, and the right panel is the predictive surface of a clustered Gaussian process.

For each choice of  $K$ , we chose the assignment of the iteration that results in the minimum LOOCV RMSE as the final assignment  $\hat{Z}$  for prediction. The right panel presents the minimum LOOCV RMSE of each choice of  $K$  in the 100 iterations, and it shows that  $K = 3$  gives the lowest LOOCV RMSE so it was selected in this example. Figure 5 demonstrates the assignments at iteration 0, 2, and 88 when  $K = 3$ . The assignment at iteration 0 represents initial assignment, which is the  $K$ -means clusters as described in Section 5.2, whose LOOCV RMSE is 0.197. The LOOCV RMSE then drops dramatically in the second iteration from 0.197 to 0.136 with only one assignment switched, that is, the point  $x_1 = 0.627, x_2 = 0.641$  is from circle to triangle cluster. With more iterations and more assignments switched, the LOOCV error decreases to 0.126 at iteration 88. The final assignment gives an intuitive explanation: the points when both of  $x_1$  and  $x_2$  are small, where the true function has a sharp change, appear to belong to the same cluster (see the circle cluster).

**6.3. Borehole function.** In the section, a borehole function, a more complex exemplar function with 8-dimensional input, is considered to examine the scalability of clustered GP. The borehole function models water flow through a borehole, and has been commonly used for testing a wide variety of methods in computer experiments because of its quick evaluation. The borehole function is given by

$$(15) \quad f(\mathbf{x}) = \frac{2\pi T_u(H_u - H_l)}{\ln(r/r_w) \left( 1 + \frac{2LT_u}{\ln(r/r_w)r_w^2 K_w} + \frac{T_u}{T_l} \right)},$$

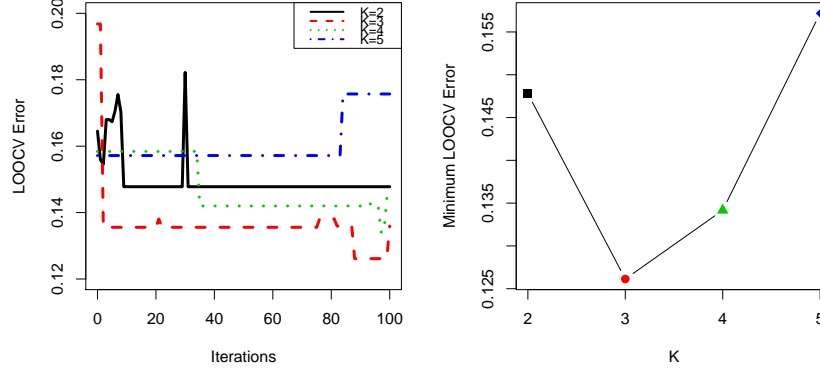


Fig 4: The LOOCV RMSEs with  $K = 2, 3, 4$  and  $5$  during the 100 iteration of the stochastic EM algorithm (left), and the minimum LOOCV RMSE of each choice of  $K$  (right).

where  $r_w \in [0.05, 0.15]$  is the radius of borehole (m),  $r \in [100, 50000]$  is the radius of influence (m),  $T_u \in [63070, 115600]$  is the transmissivity of upper aquifer ( $\text{m}^2/\text{yr}$ ),  $H_u \in [990, 1110]$  is the potentiometric head of upper aquifer (m),  $T_l \in [63.1, 116]$  is the transmissivity of lower aquifer ( $\text{m}^2/\text{yr}$ ),  $H_l \in [700, 820]$  is the potentiometric head of lower aquifer (m),  $L \in [1120, 1680]$  is the length of borehole (m), and  $K_w \in [9855, 12045]$  is the hydraulic conductivity of borehole (m/yr).

Consider  $n$  uniformly distributed input locations in the input space described above and  $n_{\text{test}} = 10,000$  random input locations in the same input space for examining prediction accuracy, whose outputs are evaluated from (15). Four methods are compared, including a stationary Gaussian process, local Gaussian process (Gramacy and Apley, 2015), multi-resolution functional ANOVA (MRFA) (Sung et al., 2019), and clustered GP. These methods are implemented using R (R Core Team, 2015) via packages `mlegp` (Dancik, 2013), `laGP` (Gramacy, 2015), `MRFA` (Sung, 2019), `clusterGP`, on a MacBook Pro laptop with 2.6 GHz Intel Core i7 and 16GB of RAM. Default settings of `mlegp`, and `MRFA` were selected, while in `laGP` we set initial values and maximum values for correlation parameters as suggested in Gramacy (2015). In `clusterGP`, the maximum numbers of iterations in the stochastic EM algorithm were set five for  $n = 1,000$  and  $n = 10,000$  and one for  $n = 100,000$  for faster computation. The maximum number of iteration can be set larger which may lead to better prediction accuracy but the computational time and storage can be quite demanding. Some remedies for the case where model fitting exceeds a user's limited budget will be discussed in Section 8. For the purpose of demonstration,  $K = n/200$  was performed for all the cases. For `laGP`, `MRFA` and `clusterGP`, 10 CPU cores were requested via `foreach` (Revolution

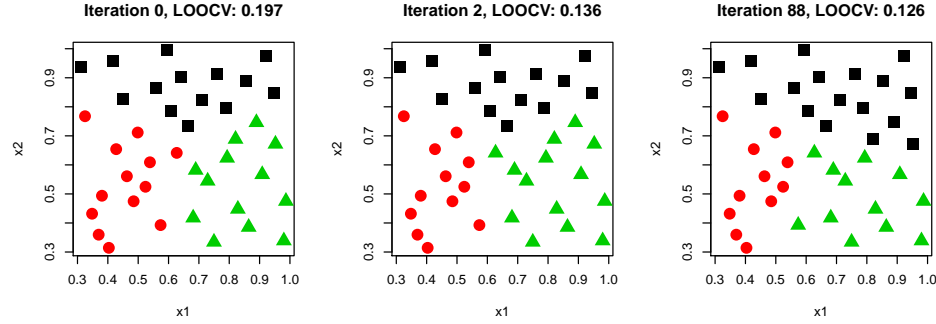


Fig 5: The cluster assignments at iteration 0, 2, and 88 of the stochastic EM algorithm and their LOOCV RMSEs.

[Analytics and Weston, 2015](#)) for parallel computing.

Table 1 shows the performance of the four methods, in terms of computation time and prediction accuracy. It can be seen that the stationary Gaussian process is only feasible when  $n = 1,000$ , while other three methods are feasible for larger  $n$ . Even when a stationary Gaussian process is feasible, the accuracy is worse than MRFA and `clusterGP`. Among the four methods, `clusterGP` has better accuracy with reasonable computation time. MRFA has slightly larger predictive errors with faster computation. On the other hand, local GP has larger predictive errors, even though the computation is faster. One may consider a different setting for local GP (e.g., the size of subsample) which may lead to better accuracy.

TABLE 1  
*Borehole function example with  $n$  training samples  $n_{\text{test}} = 10,000$  testing locations.*

Method	$n$	Fitting Time (sec.)	Prediction Time (sec.)	RMSE
mleGP	1,000	5204	24	1.0902
laGP	1,000	-	153	1.1806
	10,000	-	137	0.4149
	100,000	-	144	0.1617
MRFA	1,000	116	17	0.4668
	10,000	723	16	0.0844
	100,000	6789	18	0.0827
clusterGP	1,000	255	9	0.1124
	10,000	2950	55	0.0689
	100,000	28434	535	0.0523



**7. Solar irradiance prediction.** Predicting solar irradiance, or the power per unit area produced by electromagnetic radiation, plays a very important role in power balancing and determining the viability of potential sites for harvesting solar power. One dataset can be brought to bear on this problem is the simulations from the North American Mesoscale Forecast System (NAM) (Rogers et al., 2009), which is one of the major weather models run by the National Centers for Environmental Prediction (NCEP) for producing weather forecasts. We extract the solar irradiance (global horizontal irradiance) simulations from the NAM model at the locations of 1,535 Remote Automatic Weather Station (RAWS) (Zachariassen et al., 2003) sites in the contiguous United States. Note that the RAWS stations are not uniformly distributed. Figure 6 visualizes the available locations and their corresponding solar irradiance with the average taken over one year, which can be seen that many promising locations for solar farms are sparsely covered particularly in the Midwest. These locations of interest are considered for solar energy forecasting. Detail description of the dataset can be found in Hwang, Lu and Kim (2018) and Sun et al. (2019a). Similar to Sun et al. (2019a), here we work with average irradiance values over one year from the NAM simulations for each of 1535 spatial locations (as shown in Figure 6), and the research interest of this study is making accurate prediction for solar irradiance at those unavailable locations.

In Figure 6, it appears that some relatively high solar irradiance are measured compared to their neighborhood, such as at the location on the coordinate  $(-93.57, 45.99)$ , and some relatively low solar irradiance are measured such as at the location on the coordinate  $(-93.16, 33.69)$ . These instances may suggest that heterogeneity rather than homogeneity in the input-output relationships should be considered. The assumption of identical covariance function throughout the input domain for stationary GPs, therefore, is likely to fail and may result in poor performance, as shown in the examples of Section 6.

A clustered GP is performed on this dataset, where similar setup in Section 6.2 was used, except the maximum number of iterations in the stochastic EM algorithm was set 20 for faster computation. We first use the leave-one-out cross-validation to determine the number of clusters  $K$ . The left panel of Figure 7 shows the LOOCV RMSEs of  $K = 15, 25, 35, 45$  during the 20 iterations of the stochastic EM algorithm, and the right panel shows the minimum LOOCV RMSEs with respect to different choices of  $K$ . Based on the right panel, it appears that  $K = 35$  has the lowest LOOCV RMSE among  $K = 10, 15, 20, 25, 30, 35, 40, 45, 50$ , which suggests that  $K = 35$  is a good choice for predicting solar irradiance. Similar to the numerical study in Section 6, we chose the assignment of the iteration which results in the lowest LOOCV RMSE as the final assignment  $\hat{Z}$ . The assignment  $\hat{Z}$  is visualized in Figure 8, where the 35 clusters are presented as different colors and numbers. It appears that the assignments for the clusters are flexible that don't

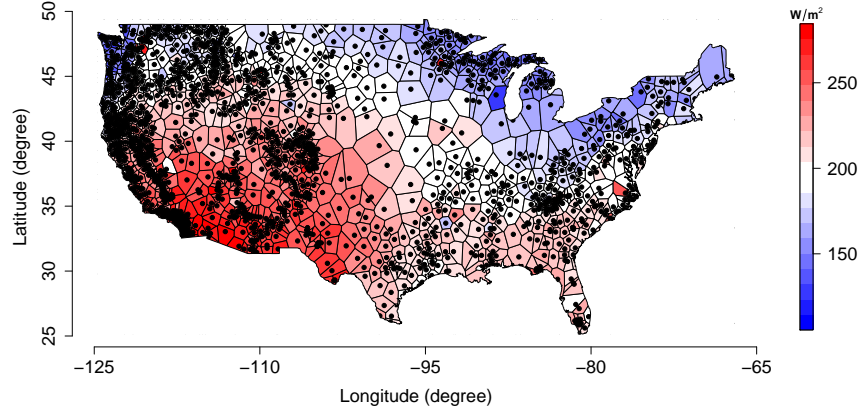


Fig 6: Solar irradiance simulation from the North American Mesoscale Forecast System (NAM). The black dots are the Remote Automatic Weather Station (RAWS) measurement sites in the contiguous United States from which the NAM simulations are extracted. The regional colors represent the solar irradiance in the subfield of a particular measurement site.

rely on linear decision boundaries. For example, the assignments of cluster 26 are mostly located on Michigan State and partially on Pennsylvania and New York State, which tells us that in those areas close to Great Lakes the solar irradiance might share the same distributions, even though they are not spatially connected. The example shows that the clustering can be useful for discovering groups and identifying interesting insight of a dataset.

To examine its prediction accuracy, we use LOOCV RMSEs as the prediction error and compare with a recent emulation method in [Sun et al. \(2019b\)](#), where they proposed a multi-resolution global/local Gaussian process emulation by extending the idea of local GP ([Gramacy and Apley, 2015](#)) by combining an ordinary “global” GP with local GPs on the residuals, and their latter work in [Sun et al. \(2019a\)](#) applied this method to the same NAM simulation data herein. [Sun et al. \(2019a\)](#) reported the LOOCV errors of the multi-resolution global/local Gaussian process emulation as well as the ordinary stationary GP which was implemented via the R package `mlegp` ([Dancik, 2013](#)). The results together with our proposed method are presented in Figure 9. The figure presents the true solar irradiance (top left) and the LOOCV predictions of a stationary GP (top right), a multi-resolution global/local GP (bottom left), and a clustered GP with  $K = 35$  (bottom right), along with their corresponding LOOCV RMSEs in the titles. It can be seen that, the stationary GP does a poor job in predicting the solar irradiance, the LOOCV predictions of which are all essentially equal which implies that almost all of the pattern remains

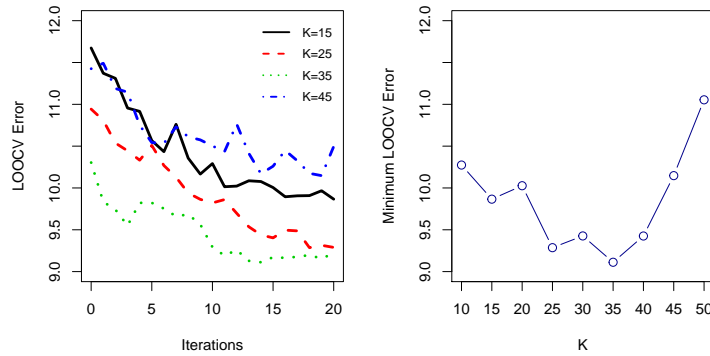


Fig 7: The LOOCV RMSEs with  $K = 15, 25, 35$  and  $45$  during the 20 iteration of the stochastic EM algorithm (left), and the minimum LOOCV RMSEs of  $K = 15, 20, 25, 30, 35, 40, 45, 50$  (right).

in the errors, which in turn gives a high LOOCV RMSE (23.20). Performances of the multi-resolution global/local GP as well as the clustered GP on the other hand are very good, the result of which may suggest that the nonstationarity should be taken into account for this dataset. Although the LOOCV predictions are visually similar, the LOOCV RMSE of the clustered GP is slightly lower than the multi-resolution global/local GP (9.11 and 9.74, respectively). In particular, it appears that the clustered GP has better prediction accuracy in the Northeast and Southeast, whereas the multi-resolution global/local GP tends to be more smooth over the whole space.

**8. Discussion.** In this paper, we proposed a clustered Gaussian process which enjoys computational advantages and tackles the nonstationarity limitations of stationary Gaussian processes. Unlike traditional clustering methods in an unsupervised way, the clusters in the clustered GP are *supervised* by the response - that is, it makes use of the response in order to partition the input domain that not only clusters the observations that have similar features, but also that have the same stationary process in the response. This clustering algorithm is implemented by a stochastic EM algorithm. Examples including the application of solar irradiance simulations show that the method not only enjoys advantages in computation and prediction accuracy, but also enables discovery of interesting insights by interpreting the clusters.

The clustered GP indicates several avenues for future research. First, the stochastic EM algorithm can be modified in an online learning fashion. That is, if the data is available in a sequential order, then instead of learning on the entire training data set at once, the algorithm can be modified to update the clusters and the best pre-

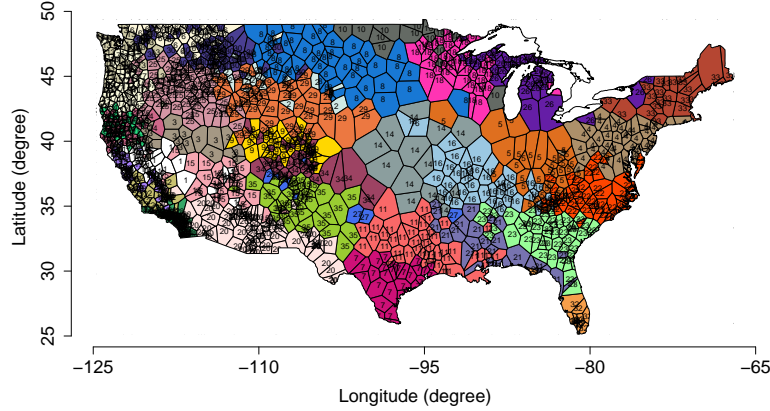


Fig 8: Visualization of the cluster assignments with  $K = 35$ .

dictor for future data at each step. For example, the solar irradiance simulations are available in every hour, so the modified algorithm can be used to update the clusters and predict future data in real time, which can save substantial computational cost and storage especially when the training sample size is extremely large.

Moreover, when the sample size is too large, due to a users limited budget (e.g., memory limitation), sub-sampling methods can be naturally applied to the clustered GP. The CURE of [Guha, Rastogi and Shim \(2001\)](#) provides an efficient algorithm for large-scale dataset for traditional clustering algorithms, which employs a combination of random sampling and partitioning, in which it also suggested the proper size of the subsample in each cluster from a theoretical perspective. It is conceivable to apply this technique to the our clustering algorithm. In addition, to reduce the prediction uncertainty on the boundary between two regions (see, for example,  $x = 10$  in Figure 2), it is conceivable to apply the idea of “patchwork” in [Park and Apley \(2018\)](#) by patching the GPs on the boundary, which can mitigate the discontinuous problem that may degrade the prediction accuracy. We leave these to our future work.

## APPENDIX

**A. Proof of Proposition 3.1.1.** For notational convention, denote  $\Sigma_j = \Phi_{\gamma_j}(X_{\mathcal{P}_j \setminus \{i\}}, X_{\mathcal{P}_j \setminus \{i\}})$  and  $W_j = Y_{\mathcal{P}_j \setminus \{i\}} - \mu_j(X_{\mathcal{P}_j \setminus \{i\}})$  for  $j = 1, \dots, K$ . Then, for any  $j \neq k$ ,

$$(A.1) \quad f_j(Y_{\mathcal{P}_j \setminus \{i\}} | X_{\mathcal{P}_j \setminus \{i\}}; \theta_j) = \frac{1}{\sqrt{2\pi \det(\Sigma_j)}} \exp \left\{ -\frac{1}{2} W_j^T \Sigma_j^{-1} W_j \right\},$$

by the fact that  $f_j$  is the probability density function of a multivariate normal distribution with parameters  $\theta_j = (\mu_j(\cdot), \sigma_j^2, \gamma_j)$ . For  $j = k$ , by partitioned matrix

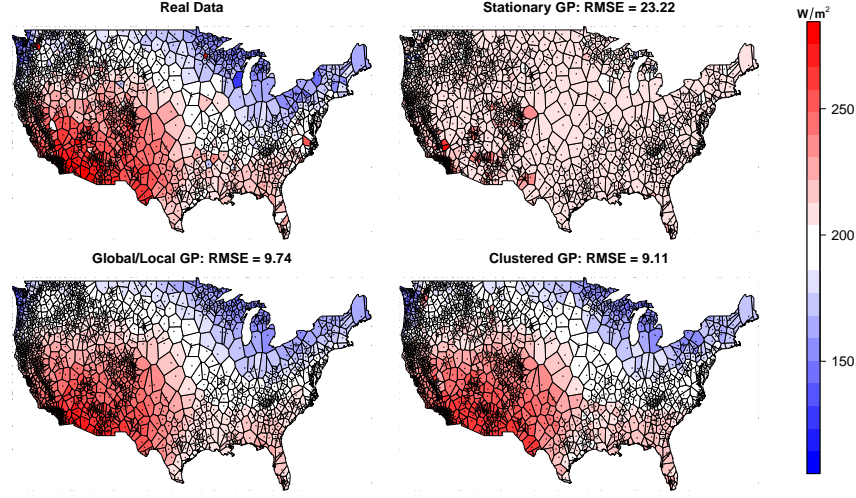


Fig 9: Comparison of solar irradiance predictions. The true solar irradiance (top left), and the LOOCV predictions of a stationary GP (top right), a multi-resolution global/local GP (bottom left), and a clustered GP with  $K = 35$  (bottom right) are presented, along with their corresponding LOOCV RMSEs in the figure titles.

inverse and determinant formulas,

$$f_k(Y_{\mathcal{P}_k \cup \{i\}} | X_{\mathcal{P}_k \cup \{i\}}) = \frac{1}{\sqrt{2\pi \det \left( \begin{bmatrix} \Sigma_k & r_{i,-i}^T \\ r_{i,-i} & \sigma_k^2 \end{bmatrix} \right)}} \exp \left\{ -\frac{1}{2} \begin{bmatrix} W_k \\ y_i - \mu_k(x_i) \end{bmatrix}^T \begin{bmatrix} \Sigma_k & r_{i,-i}^T \\ r_{i,-i} & \sigma_k^2 \end{bmatrix}^{-1} \begin{bmatrix} W_k \\ y_i - \mu_k(x_i) \end{bmatrix} \right\} \quad (\text{A.2})$$

$$= f_k(Y_{\mathcal{P}_k \setminus \{i\}} | X_{\mathcal{P}_k \setminus \{i\}}) \times \frac{1}{\sqrt{(\sigma_k^*)^2}} \exp \left\{ -\frac{1}{2} (y_i - \mu_k^*)^2 / (\sigma_k^*)^2 \right\},$$

where  $r_{i,-i} = \Phi_{\gamma_k}(x_i, X_{\mathcal{P}_k \setminus \{i\}})$ ,  $\mu_k^* = \mu_k(x_i) + r_{i,-i} \Sigma_k^{-1} W_k$  and  $(\sigma_k^*)^2 = \sigma_k^2 (1 - r_{i,-i} \Sigma_k^{-1} r_{i,-i}^T)$ .

Therefore, combining (10), (A.1) and (A.2),

$$\begin{aligned} f(z_i = k | X, Y, Z_{-i}) &\propto f_k(Y_{\mathcal{P}_k \cup \{i\}} | X_{\mathcal{P}_k \cup \{i\}}; \theta_k) \prod_{j \neq k} f_j(Y_{\mathcal{P}_j \setminus \{i\}} | X_{\mathcal{P}_j \setminus \{i\}}; \theta_j) g_k(x_i; \varphi_k) \\ &= \prod_{k=1}^K f_k(Y_{\mathcal{P}_k \setminus \{i\}} | X_{\mathcal{P}_k \setminus \{i\}}; \theta_k) \exp \left\{ -\frac{1}{2} (y_i - \mu_k^*)^2 / (\sigma_k^*)^2 \right\} g_k(x_i; \varphi_k) \\ &\propto \phi((y_i - \mu_k^*) / \sigma_k^*) g_k(x_i; \varphi_k). \end{aligned}$$

### B. Stochastic EM Algorithm for Clustered Gaussian Process.

#### Initialization:

Set  $K$  clusters with random memberships  $\{z(x_i)\}_{i=1}^n$

Set  $\mathcal{P}_k \leftarrow \{i : z(x_i) = k\}$  for each  $k$

Set initial parameters  $\theta_k = \{\mu_k(\cdot), \sigma_k^2, \gamma_k\}$  and  $\varphi_k$  for  $k = 1, \dots, K$

#### Stochastic E-Step:

For  $i = 1$  to  $i = n$ ,

For  $k = 1$  to  $K$  do parallel,

$$\begin{aligned} \mu_k^* &\leftarrow \mu_k(x_i) + \Phi_{\gamma_k}(x_i, X_{\mathcal{P}_k \setminus \{i\}}) \Phi_{\gamma_k}(X_{\mathcal{P}_k \setminus \{i\}}, X_{\mathcal{P}_k \setminus \{i\}})^{-1} (Y_{\mathcal{P}_k \setminus \{i\}} - \mu_k(X_{\mathcal{P}_k \setminus \{i\}})) \\ (\sigma_k^*)^2 &\leftarrow \sigma_k^2 (1 - \Phi_{\gamma_k}(x_i, X_{\mathcal{P}_k \setminus \{i\}}) \Phi_{\gamma_k}(X_{\mathcal{P}_k \setminus \{i\}}, X_{\mathcal{P}_k \setminus \{i\}})^{-1} \Phi_{\gamma_k}(X_{\mathcal{P}_k \setminus \{i\}}, x_i)) \\ p_{ik} &\leftarrow \frac{\phi((y_i - \mu_k^*)/\sigma_k^*) g_k(x_i; \varphi_k)}{\sum_{k=1}^K \phi((y_i - \mu_k^*)/\sigma_k^*) g_k(x_i; \varphi_k)} \end{aligned}$$

Draw  $z$  from a random multinomial cluster assignment with probabilities  $(p_{i1}, \dots, p_{iK})$

Update  $z(x_i) \leftarrow z$

Update  $\mathcal{P}_k \leftarrow \{i : z(x_i) = k\}$  for each  $k$

#### M-Step:

For  $k = 1$  to  $K$  do parallel,

Update  $\theta_k \leftarrow \arg \max_{\theta_k} \log f_k(Y_{\mathcal{P}_k} | X_{\mathcal{P}_k}; \theta_k) \pi(\theta_k)$

Update  $\{\varphi_k\}_{k=1}^K \leftarrow \arg \max_{\varphi} \sum_{k=1}^K \left( \sum_{i \in \mathcal{P}_k} \log g_k(x_i; \varphi_k) + \log \pi(\varphi_k) \right)$

**Iteration:** Iterate stochastic E-step and M-step until some stopping rule is met.

**Output**  $\{z(x_i)\}_{i=1}^n, \{\theta_k, \varphi_k\}_{k=1}^K$

**C. One-Dimensional Examples.** Two more one-dimensional examples of Section 6.1 are presented here. Consider an example from [Xiong et al. \(2007\)](#), where the true function is

$$f(x) = \sin(30(x - 0.9)^4) \cos(2(x - 0.9)) + (x - 0.9)/2$$

and 17 unequally spaced points from  $[0, 1]$  are chosen to evaluate. Similarly, the top panels of Figure 10 show that the clustered GP (right) outperforms the stationary GP (left) in terms of prediction accuracy and uncertain quantification. The two clusters are separated at location around  $x = 0.40$ . In particular, the predictor in the region  $[0.42, 1.00]$  has better prediction accuracy with much smaller prediction uncertainty. The same argument applies to this example: the constant mean and variance assumptions are violated in this function so the stationary GP results in the erratic prediction in the region  $[0.42, 1.00]$ .

Lastly, consider the inhomogeneous smooth function in [Montagna and Tokdar \(2016\)](#),

$$f(x) = \sin(x) + 2 \exp(-30x^2),$$

and 15 unequally spaced points from  $[-2, 2]$  are chosen to evaluate. The bottom panel of Figure 10 demonstrates a stationary Gaussian process (left), where the

prediction mean curve has large oscillations with confidence intervals except the tall peak in the middle. This is due to the rippling effect of the discovery of a tall peak, and [Montagna and Tokdar \(2016\)](#) called the phenomenon a *spline tension* effect in the predictor form. The clustered GP (right) overcomes the issue by separating the input locations into three clusters and fits a stationary GP in each cluster. The result shows that the prediction mean curve quite matches the true curve with a narrower confidence band.

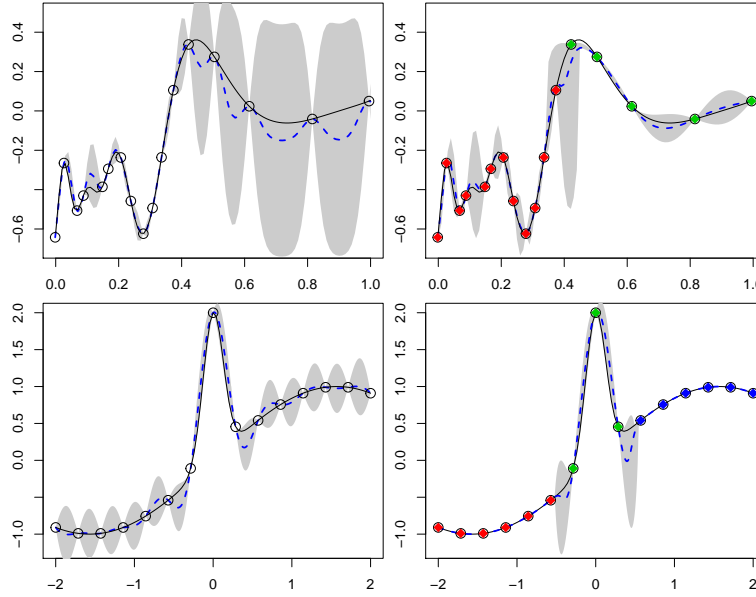


Fig 10: One-dimensional synthetic data. The left and right panels illustrate predictors by a stationary Gaussian process and a clustered Gaussian process, respectively. Black line is the true function, black circles are input locations, and blue dotted lines are the predictors, with the gray shaded region providing a pointwise 95% confidence band. Red, green, and blue dots in the right panels represent different clusters.

## References.

- REVOLUTION ANALYTICS and WESTON, S. (2015). foreach: Provides Foreach Looping Construct for R R package version 1.4.3.
- BA, S. and JOSEPH, V. R. (2012). Composite Gaussian process models for emulating expensive functions. *The Annals of Applied Statistics* **6** 1838–1860.
- BUI-THANH, T., GHATTAS, O. and HIGDON, D. (2012). Adaptive Hessian-based nonstationary Gaussian process response surface method for probability density approximation with application to Bayesian solution of large-scale inverse problems. *SIAM Journal on Scientific Computing* **34** A2837–A2871.



- CELEUX, G. and DIEBOLT, J. (1985). The SEM algorithm: a probabilistic teacher algorithm derived from the EM algorithm for the mixture problem. *Computational Statistics Quarterly* **2** 73–82.
- DANCIK, G. M. (2013). mlegp: Maximum Likelihood Estimates of Gaussian Processes R package version 3.1.4.
- EFRON, B. and TIBSHIRANI, R. (1997). Improvements on cross-validation: the 632+ bootstrap method. *Journal of the American Statistical Association* **92** 548–560.
- FANG, K.-T., LI, R. and SUDJANTO, A. (2005). *Design and Modeling for Computer Experiments*. CRC Press.
- FURRER, R., GENTON, M. G. and NYCHKA, D. (2006). Covariance tapering for interpolation of large spatial datasets. *Journal of Computational and Graphical Statistics* **15** 502–523.
- GRAMACY, R. B. (2015). laGP: large-scale spatial modeling via local approximate Gaussian processes in R. *Journal of Statistical Software* (available as a vignette in the laGP package).
- GRAMACY, R. B. and APLEY, D. W. (2015). Local Gaussian process approximation for large computer experiments. *Journal of Computational and Graphical Statistics* **24** 561–578.
- GRAMACY, R. B. and LEE, H. K. H. (2008). Bayesian treed Gaussian process models with an application to computer modeling. *Journal of the American Statistical Association* **103** 1119–1130.
- GRAMACY, R. B. and LEE, H. K. H. (2009). Adaptive design and analysis of supercomputer experiments. *Technometrics* **51** 130–145.
- GUHA, S., RASTOGI, R. and SHIM, K. (2001). Cure: an efficient clustering algorithm for large databases. *Information Systems* **26** 35–58.
- HAALAND, B. and QIAN, P. Z. G. (2011). Accurate emulators for large-scale computer experiments. *The Annals of Statistics* **39** 2974–3002.
- HARVILLE, D. A. (1998). *Matrix Algebra from a Statistician's Perspective*. Springer, New York, NY.
- HIGDON, D. et al. (2002). Space and space-time modeling using process convolutions. *Quantitative Methods for Current Environmental Issues* **3754** 37–56.
- HIGDON, D., SWALL, J. and KERN, J. (1999). Non-stationary spatial modeling. *Bayesian Statistics* **6** 761–768.
- HWANG, Y., LU, S. and KIM, J.-K. (2018). Bottom-up estimation and top-down prediction: Solar energy prediction combining information from multiple sources. *Annals of Applied Statistics* **12** 2096–2120.
- KIM, H.-M., MALLICK, B. K. and HOLMES, C. C. (2005). Analyzing nonstationary spatial data using piecewise Gaussian processes. *Journal of the American Statistical Association* **100** 653–668.
- KOHAVER, R. (1995). A study of cross-validation and bootstrap for accuracy estimation and model selection. In *Proceedings of International Joint Conference on Artificial Intelligence* 1137–1145.
- MONTAGNA, S. and TOKDAR, S. T. (2016). Computer emulation with nonstationary Gaussian processes. *SIAM/ASA Journal on Uncertainty Quantification* **4** 26–47.
- MORRIS, M. D. and MITCHELL, T. J. (1995). Exploratory designs for computational experiments. *Journal of Statistical Planning and Inference* **43** 381–402.
- NGUYEN-TUONG, D. and PETERS, J. (2011). Model learning for robot control: a survey. *Cognitive processing* **12** 319–340.
- NIELSEN, S. F. et al. (2000). The stochastic EM algorithm: estimation and asymptotic results. *Bernoulli* **6** 457–489.
- NYCHKA, D., BANDYOPADHYAY, S., HAMMERLING, D., LINDGREN, F. and SAIN, S. (2015). A multi-resolution Gaussian process model for the analysis of large spatial data sets. *Journal of Computational and Graphical Statistics* **24** 579–599.
- PACIOREK, C. J. and SCHERVISH, M. J. (2006). Spatial modelling using a new class of nonstationary covariance functions. *Environmetrics* **17** 483–506.



- PARK, C. and APLEY, D. (2018). Patchwork kriging for large-scale gaussian process regression. *The Journal of Machine Learning Research* **19** 269–311.
- PLUMLEE, M. (2014). Fast prediction of deterministic functions using sparse grid experimental designs. *Journal of the American Statistical Association* **109** 1581–1591.
- PLUMLEE, M. and APLEY, D. W. (2017). Lifted Brownian kriging models. *Technometrics* **59** 165–177.
- QUINONERO-CANDELA, J. and RASMUSSEN, C. E. (2005). A unifying view of sparse approximate Gaussian process regression. *Journal of Machine Learning Research* **6** 1939–1959.
- RASMUSSEN, C. E. and GHAHRAMANI, Z. (2002). Infinite mixtures of Gaussian process experts. In *Advances in neural information processing systems* 881–888.
- RASMUSSEN, C. E. and WILLIAMS, C. K. (2006). *Gaussian processes for machine learning* **1**. MIT press Cambridge.
- ROGERS, E., DIMEGO, G., BLACK, T., EK, M., FERRIER, B., GAYNO, G., JANJIC, Z., LIN, Y., PYLE, M., WONG, V. et al. (2009). The NCEP North American mesoscale modeling system: Recent changes and future plans. In *23rd Conference on Weather Analysis and Forecasting/19th Conference on Numerical Weather Prediction*, Omaha, NE.
- SANG, H. and HUANG, J. Z. (2012). A full scale approximation of covariance functions for large spatial data sets. *Journal of the Royal Statistical Society: Series B* **74** 111–132.
- SANTNER, T. J., WILLIAMS, B. J. and NOTZ, W. I. (2018). *The Design and Analysis of Computer Experiments*, 2 ed. Springer-Verlag New York.
- SNELSON, E. and GHAHRAMANI, Z. (2006). Sparse Gaussian processes using pseudo-inputs. In *Advances in Neural Information Processing Systems* 1257–1264.
- STEIN, M. L. (2012). *Interpolation of Spatial Data: Some Theory for Kriging*. Springer Science & Business Media.
- SUN, F., GRAMACY, R. B., HAALAND, B., LU, S. and HWANG, Y. (2019a). Synthesizing simulation and field data of solar irradiance. *Statistical Analysis and Data Mining*. to appear.
- SUN, F., GRAMACY, R. B., HAALAND, B., LAWRENCE, E. and WALKER, A. (2019b). Emulating satellite drag from large simulation experiments. *SIAM/ASA Journal on Uncertainty Quantification*.
- SUNG, C.-L. (2019). MRFA: Fitting and Predicting Large-Scale Nonlinear Regression Problems using Multi-Resolution Functional ANOVA (MRFA) Approach R package version 0.4.
- SUNG, C.-L., WANG, W., PLUMLEE, M. and HAALAND, B. (2019). Multi-resolution functional ANOVA for large-scale, many-input computer experiments. *Journal of the American Statistical Association*. to appear.
- R CORE TEAM (2015). R: A Language and Environment for Statistical Computing R Foundation for Statistical Computing, Vienna, Austria.
- TITSIAS, M. (2009). Variational learning of inducing variables in sparse Gaussian processes. In *Artificial Intelligence and Statistics* 567–574.
- TRESP, V. (2001). Mixtures of Gaussian processes. In *Advances in neural information processing systems* 654–660.
- XIONG, Y., CHEN, W., APLEY, D. and DING, X. (2007). A non-stationary covariance-based Kriging method for metamodeling in engineering design. *International Journal for Numerical Methods in Engineering* **71** 733–756.
- ZACHARIASSEN, J., ZELLER, K. F., NIKOLOV, N. and MCCLELLAND, T. (2003). A review of the forest service remote automated weather station (RAWS) network. *General Technical Report*. No. RMRS-GTR-119.